SAND99-0226C

DEEP X-RAY LITHOGRAPHY BASED FABRICATION OF RARE-EARTH BASED PERMANENT MAGNETS AND THEIR APPLICATIONS TO MICROACTUATORS

Todd R. Christenson, Terry J. Garino, Eugene L. Venturini
Sandia National Laboratories
P.O. Box 5800
Albuquerque, NM 87185-0329

Abstract

Precision high aspect-ratio micro molds constructed by deep x-ray lithography have been used to batch fabricate accurately shaped bonded rare-earth based permanent magnets with features as small as 5 microns and thicknesses up to 500 microns. Maximum energy products of up to 8 MGOe have been achieved with a 20%/vol. epoxy bonded melt-spun isotropic $Nd_2Fe_{14}B$ powder composite. Using individually processed sub-millimeter permanent sections multipole rotors have been assembled. Despite the fact that these permanent magnet structures are small, their magnetic field producing capability remains the same as at any scale. Combining permanent magnet structures with soft magnetic materials and micro-coils makes possible new and more efficient magnetic microdevices.

INTRODUCTION

Permanent magnets, and in particular rare-earth based permanent magnets, have fundamental properties that make their use on the microscale highly attractive. The most interesting of these properties is that the magnetization of a permanent magnet is independent of scale. Stated another way, the field strength of a permanent magnet does not depend on the size of the magnet. The advantage of a permanent magnet relative to an electromagnet has been pointed out with particular emphasis by Halbach who stated the point in the following way: "... when it is necessary that a magnetically significant dimension of a magnet is very small, a permanent magnet will always produce higher fields than an electromagnet ... with permanent magnets one can reach regions of parameter space that are not accessible with any other technology."(1) This situation occurs due to an inverse linear scaling dependence of an electromagnetic coil brought about by current density constraints due to thermal and electromigration limitations. Coils utilizing superconductors share the same scaling relationship which arises due to a similar critical current density limit.

To quantify at what reduced dimension a permanent magnet begins to posses significantly improved performance compared to a coil is in general not possible, as this is a function of many parameters of a particular application. An estimate for a typical

DISCLAIMER

microactuator application involving a "horseshoe" geometry is presented here. By comparing the flux generating capabilities of an equivalent volume of permanent magnet and coil an expression for the ratio, γ_H, of the two is found to have a dependence as given by equation [1]. In this equation γ_H is the ratio of magnetic field produced by the

$$\gamma_H = \frac{B_r/\mu_m}{2\alpha\mu_0 t_c J_{max}} \qquad [1]$$

permanent magnet to that produced by the coil where B_r is the remanent flux density of the magnet material, μ_m is its recoil permeability, α is the coil winding efficiency, μ_0 is the permeability of free space, t_c is the coil thickness (or describing dimension normal to the flux path) and J_{max} is the maximum current density of the coil wire. This relationship assumes the use of a magnetic material with a linear demagnetization curve which is possessed by rare-earth based permanent magnets. The linear dimensional dependence of the coil is readily seen. Equation [1] is plotted in Fig. 1 with various values of J_{max} and shows that large benefits occur with permanent magnet flux generation in this case below about several millimeters.

The permanent magnet advantages are most fully exploited if in particular rare-earth based permanent magnets (REPM) are considered. These types of magnets of the Sm-Co and Nd-Fe-B family possess very large magnetization per unit volume with high intrinsic coercivities. The large remanent magnetization yields high flux densities which is important for magnetic microactuators where the pressure developed is proportional to the square of the magnetic flux density. The large coercivity makes the REPM highly resistant to demagnetization by external or internal demagnetizing fields. This property reveals itself in the linearity of the B vs. $\mu_0 H$ second quadrant behavior which allows the magnet to be immersed in fields greater than remanence. The result is a nearly constant magnetization in opposing fields as high as 15,000 Oersted thereby establishing a nearly ideal mmf (magnetomotive force) source much like a "magnetic battery."(2) This property of REPM allows for relatively straightforward design of novel magnetic structures which can generate very finely tailored magnetic fields (3,4). The last advantage to be mentioned for permanent magnets is of particular value to static magnetic devices which is that there are no ohmic coil losses or currents required to sustain the magnetic field.

Implementing multipole REPM based structures on the microscale, however, immediately raises the problem of generating the necessary magnetizing field. For typical REPM materials this required field is in excess of 35,000 Oe. As a multipole structure becomes smaller, generating this required alternating high intensity magnetizing field with a magnetizing fixture becomes impractical and eventually not possible. For this reason an assembly technique based on individual precision microfabricated REPM sections is proposed. The fabrication approach to be explained is based on deep x-ray lithography (DXRL) techniques which can facilitate the necessary precision. Microscale assembly techniques that have been further implemented to generate three dimensional microstructures (5) provide the basis for the required assembly.

The resulting permanent magnet structures when augmented with appropriately constructed soft (highly permeable) magnetic materials as well as suitable micro coils form the basis for a more efficient magnetic microactuator technology.

This situation has been appreciated by several previous reports (6,7) which used conventionally machined rare-earth permanent magnets in combination with silicon micromachining. Methods to electroform (8) and pattern ferrite embedded photo polymers (9) have also been reported. What is evident from these studies is the complex implementation problems inherent in batch integration of high performance permanent magnets which must be addressed for MEMS (Micro Electro Mechanical Systems) applications.

DXRL BASED FABRICATION OF REPM

Deep x-ray lithography provides a superb tool for the fabrication of high aspect-ratio microstructures. (10,11) The process creates a mold form in PMMA (poly methyl methacrylate), the preferred deep x-ray photoresist, with nearly perfect prismatic features that possess dimensions down to a few microns, thicknesses up to several millimeters, and tolerances below one micron. This mold form is typically transferred to a complementary metal structure via electroforming. The mold may, however, be used to press other materials as has been demonstrated with ceramics (12,13) which forms the basis for filling DXRL defined molds using powder metallurgy and expands the available materials over electroformable materials considerably. This type of micromold filling process is what is proposed as a basis for precision micro magnet fabrication to reach the ultimate goal of perfectly replicated REPM structures.

A common figure of merit for permanent magnets is their maximum energy product which directly pertains to actuator performance and efficiency. Rare-earth based permanent magnets possess the highest available energy products of over 40 MGOe (Mega-Gauss-Oersted, 1 MGOe = $100/4\pi$ kJ/m^3). These energy products refer to fully dense sintered forms that present a problem for direct replication from PMMA molds due to an unacceptable volume shrink occurring at the required high sintering temperatures. A less involved approach, however, is possible by incorporating a rare-earth magnet powder with a binder such as an epoxy to produce bonded or composite magnets. This type of magnet is experiencing extremely rapid commercial growth due to its ability to be molded and thus inexpensively form precise shapes much more easily than its brittle fully dense REPM counterpart. The concession is a reduction in remanence and thus energy product due to the reduced density. Nevertheless, energy products of bonded REPM of 10 MGOe are common for isotropic powder which is still well in excess of that of ferrites or ceramic magnets. A summary of maximum energy densities possessed by various magnet materials is listed in Table I.

A variety of techniques have been investigated to form bonded REPM directly from a DXRL defined PMMA mold. A basic preferred sequence is outlined in the

Table I. Permanent Magnet Maximum Energy Product Comparison

	Material	*Energy Product - MGOe (typ.)*	*kJ/m³ (typ.)*
	Carbon steel	0.25	2
	Alnico	5 - 9 (5.5)	44
	Ferrite (Ceramic)	1 - 4.5 (3.5)	28
	Bonded Ferrite	0.3 - 2 (0.6)	5
	PtCo	7-9	64
Rare Earth Based	Sm-Co	6 - 31 (26)	208
	Nd-Fe-B	22 - 48 (40)	320
	Bonded Nd-Fe-B	6-19 (10)	80

process cross sections of Fig. 2. A DXRL defined PMMA mold is provided on a substrate coated with a suitable sacrificial material such as copper. An unmagnetized powder/epoxy mixture is then applied to the substrate while in a low viscosity state by calendering and pressing with additional centrifugal force being sometimes rendered. Powder particle sizes of less than 20 microns are commonly used with meltspun isotropic $Nd_2Fe_{14}B$ powder being used predominantly.(14) After curing in a press with a typical pressure of 10 ksi, the substrate with pressed composite is lapped to thickness. The entire substrate of permanent magnets is then subjected to a magnetizing field of at least 35 kOe in the desired orientation thereby batch magnetizing all magnets. The PMMA is removed with a solvent to which the epoxy binder is resistant and the permanent magnets are released by undercutting the underlying sacrificial layer.

RESULTS

Bonded REPM with dimensions as small as 5 microns have been made using the DXRL based molds. Results are shown in Fig. 3 for a variety of geometry at a magnet thickness of 200 microns. Most notable is the accurate reproduction of the PMMA sidewall. Distortion is present in the SEM photographs since the magnets are magnetized. This artifact is made evident by using a different accelerating voltage as shown in a) and b) where the 5kV image shows more distortion.

Figure 4 shows the full measured hysteresis loop for isotropic $Nd_2Fe_{14}B$ powder with 20% by volume epoxy that was measured using a squid magnetometer. The remanent magnetization is 0.63 T and the coercivity is 1.4 T with a maximum energy product of near 8 MGOe. The dependence of maximum energy product on epoxy fraction is graphed in Fig. 5. A 30% epoxy volume is used most frequently as this yields magnets with sufficient mechanical strength to be handled during assembly. Greater epoxy fractions increase mechanical strength while further reducing energy product. The maximum energy product for this powder alone without epoxy is 10 MGOe. The results for the smallest volume magnet that was measured are given in Fig. 6. Although still a

strong magnet, it is suspected that a uniform composite density was not achieved as is suggested by the sidewall of the magnets shown in Fig. 3 d). Further improvement of the energy product can be accomplished by utilizing anisotropic powder which in bonded form can attain energy products up to 19 MGOe. Work is being conducted to incorporate these powders which requires pressing in an orienting magnetic field of about 1 T.

APPLICATIONS

Two broad areas of application are of interest for the DXRL defined permanent magnets. The first involves microactuators and is demonstrated by the magnet geometry depicted in Fig. 3. The quadrant shapes are patterned in a way to identify the direction of magnetization resulting from the batch magnetizing step after they are released. Subsequent to release they are assembled together in a cylinder which comprises a multipole rotor for a brushless DC motor. This assembly is shown in Fig. 7 for a 4-pole rotor intended for use with a 9-pole stator which surrounds the permanent magnet rotor. Since the torque developed by such a motor is directly proportional to the number of permanent magnet poles (as long as adjacent pole – pole fringing remains low) further performance improvements may be made by accommodating an 8 pole rotor which has been implemented by using the octant shaped segments shown in Fig. 3c). More complex geometry may profit from assembly approaches involving successive batch wafer transfer. With the use of permanent magnets magnetic microactuators exhibit improved efficiency as has been demonstrated by conventionally machined miniature brushless DC motors.(15) A major class of devices including micro generators and servo systems is also realizable.

The second area of application involves static magnetic structures such as miniature Halbach arrays (or magic rings) and field reinforcing structures that utilize intricate multipole elements. This category also includes charged particle focussing arrangements. Fig. 3c) shows some trapezoidal shapes which when assembled in an array fashioned in a manner depicted in Fig. 8 constitute a Halbach array. Partial arrow shapes on the trapezoidal shapes in Fig. 3c) indicate magnetization direction. Two factors result from this arrangement. The first is that the field generated in the inside region is uniform, and the second is that this inside field is magnified by an amount indicated in equation [2] where B_r is the remanent magnetization, and r_0 and r_i are the

$$B_{inner} = B_r \ln\left(\frac{r_0}{r_i}\right) \qquad [2]$$

respective outer and inner array radii. This practically allows for an increase in magnetic flux density of nearly 2 which increases the magnetic pressure fourfold and makes possible pressures in excess of 300 psi. Such scale independent forces become extremely compelling for use in microactuators. The use of cylindrical Halbach arrays has also been recognized for conventional scale permanent magnet motors. Such an array also has application to microsensors which need a static magnetic bias field such as for magnetically excited flexural plate wave resonators.(16)

Another miniature permanent magnet application is in compensating for a MEMS scaling problem involving springs. Mechanical spring constants scale inversely proportional to length and thus spring geometry can become relatively large on the microscale to yield sufficiently soft springs. The very nearly constant second quadrant magnetization of REPMs leads to interacting behavior very much like mechanical springs with linear spring constants. If permanent magnets are integrated into a spring geometry to produce a repulsion force, this force may be used to subtract from the mechanical spring force resulting in a decreased effective spring constant as described by equation

$$F_s = (k_S - k_{PM})x \qquad [3]$$

[3] where k_S is the mechanical spring constant and k_{PM} is the "spring constant" due to the permanent magnet arrangement. One possible arrangement is drawn in Fig. 9. A technique is thereby demonstrated that uses permanent magnets to negate unwanted scaling behavior.

CONCLUSIONS

The use of permanent magnets on the microscale is compelling due to their scaling properties. This is particularly true for rare-earth based permanent magnets which due to their high demagnetization resistance are amenable to flat and nearly arbitrary aspect-ratio. Deep x-ray lithography based processing provides a convenient means to fabricate a multitude of miniature REPMs in a simultaneous batch manner which further facilitate efficient microactuators and other novel microdevices. The nature of multipole REPM structures necessitates an assembly approach which would benefit from batch assembly techniques.

ACKNOWLEDGMENTS

The author would like to acknowledge B. Ritchey for the SEM photography and D. Berry for the optical photography. This work was performed at Sandia National Laboratories, a multi-program laboratory operated by the Sandia corporation, a Lockheed Martin Company, for the United States Department of Energy under contract #DE-AC04-94AL85000.

REFERENCES

1. K. Halbach, in High Performance Permanent Magnet Materials/1987, S.G. Sankar, J.F. Herbst, and N.C. Koon, Editors, **96**, p. 259, Materials Research Society Symposium Proceedings, Pittsburgh, PA (1987).
2. K.J. Strnat, Proc. of the IEEE, **78**, 923, (1990).
3. M.G. Abele, Structures of Permanent Magnets: Generation of Uniform Fields, Wiley Interscience, New York (1993).

4. H. A. Leupold, in Rare-Earth Iron Permanent Magnets, J.M.D. Coey, Editor, **54**, p. 381, Monographs on the Physics and Chemistry of Materials, Clarendon Press, Oxford (1996).
5. H. Guckel, T. Christenson, and K. Skrobis, J. Micromech. Microeng., **2**, 225 (1992).
6. R.L. Smith, R.W. Bower, and S.D. Collins, Sensors and Actuators A, **24**, 47 (1990).
7. B. Wagner and W. Benecke, in Proc. of IEEE Micro Electro Mechanical Systems (MEMS '91), p. 27 (1991).
8. T.K. Liakopolous, W. Zhang, and C.H. Ahn, Proc. of IEEE Micro Electro Mechanical Systems (MEMS '96), p. 79 (1996).
9. L.K. Lagorce and M.G. Allen, Proc. of IEEE Micro Electro Mechanical Systems (MEMS '96), p. 85 (1996).
10. H. Guckel, Proc. of the IEEE, **86**, 1586 (1998).
11. T.R. Christenson and H. Guckel, in Proceedings SPIE Micromachining and Microfabrication Process Technology, **2639**, 134 (1995).
12. H.-J.Ritzhaupt-Kleissl, W. Bauer, E. Günther, J. Laubersheimer, J. Haußelt, Microsystem Technologies, **2**, No. 3, p.1301 (1996).
13. V. Pioter, T. Hanemann, R. Ruprecht, A. Thies, J. Haußelt, in Proc. Of SPIE Micromachining and Microfabrication Process Technology III, **3223**, p. 91 (1997).
14. Magnequench International Inc., Neodymium-Iron-Boron Powder Data Sheet.
15. M. Jufer, C. Péclat, A. Birkicht, in Proc. Of 26th Symposium on Incremental Motion Control Systems and Devices, 159 (1997).
16. S.J. Martin, S.A. Butler, J.J. Spates, M.S. Mitchell, and M.K. Schubert, J. Appl. Phys., **83** (9), p. 4589 (1998).

FIGURES

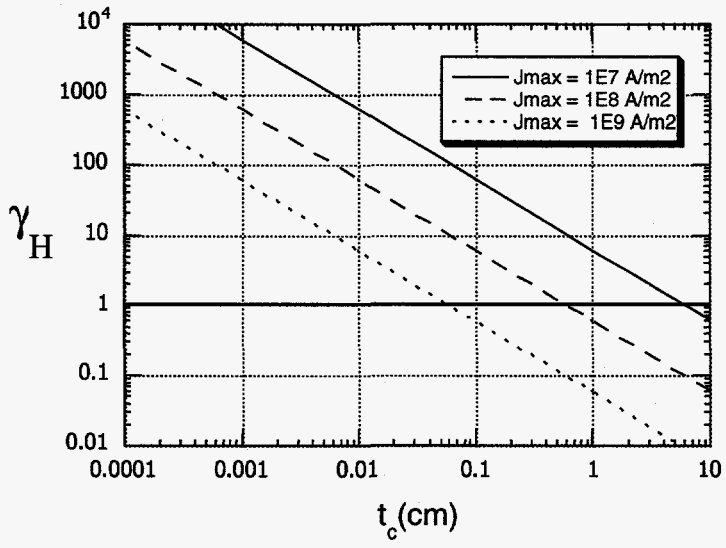

Fig. 1 Equation [1] plotted for various values of J_{max} with B_r=1.2 T, μ_m=1.05, α=0.75, and $\mu_0=4\pi(10)^{-7}$ Hy/m. This plot is intended only as a rough gauge of the trade-off involved between a permanent magnet and a coil in generating a static magnetic field.

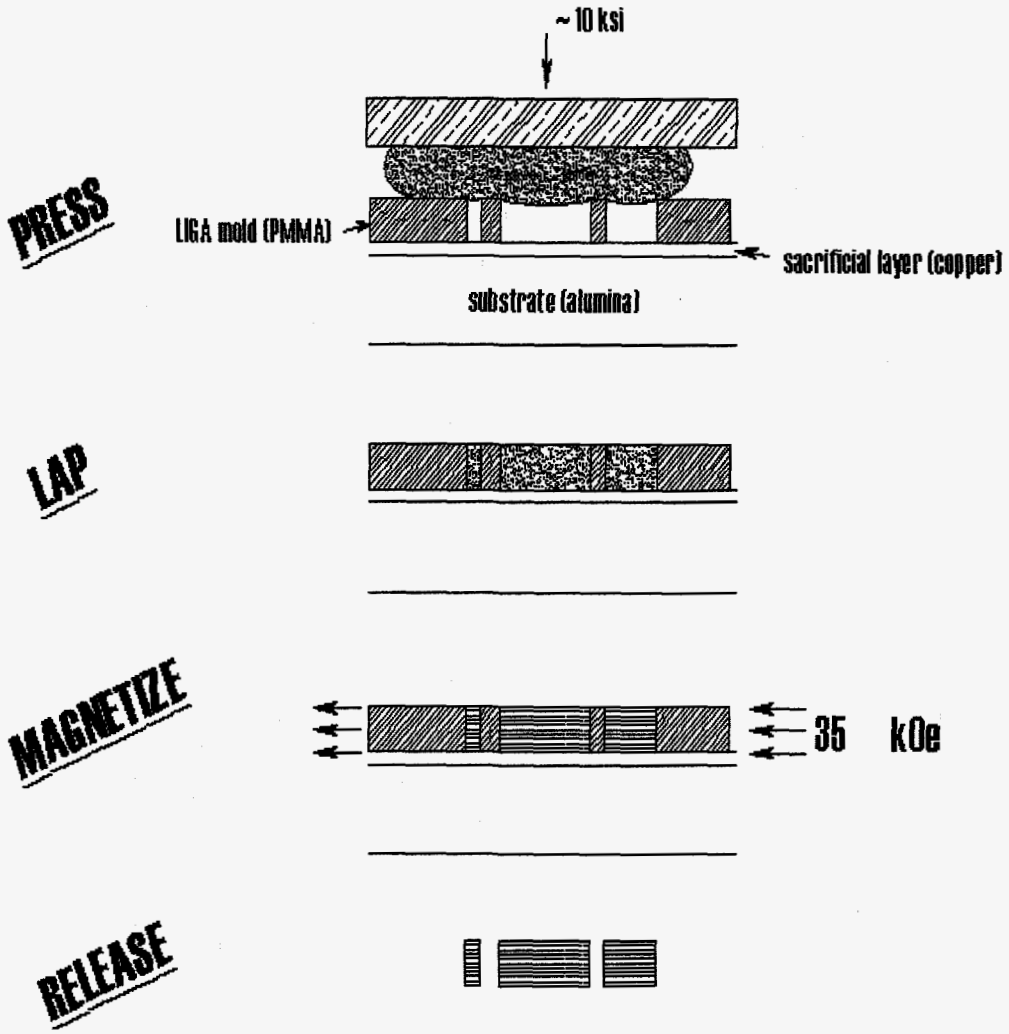

Fig. 2 DXRL based bonded REPM process.

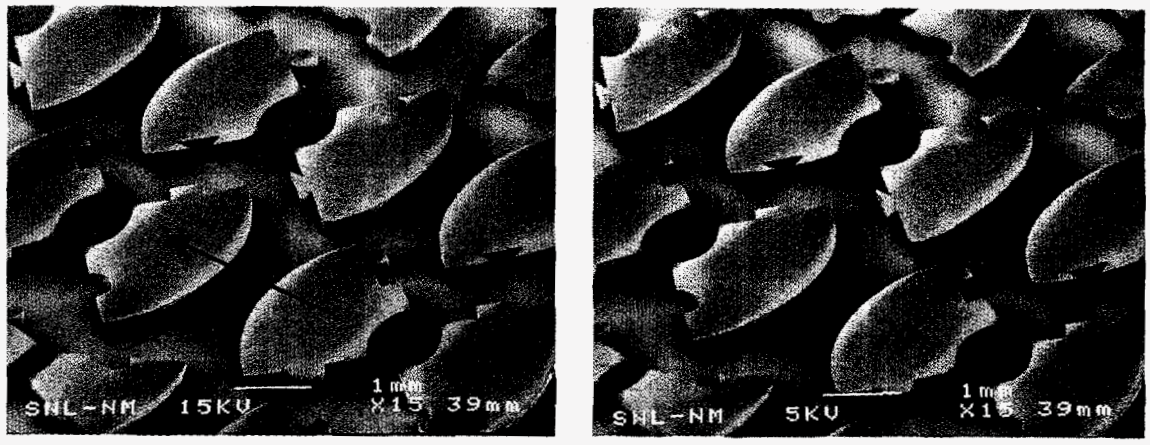

a) b)

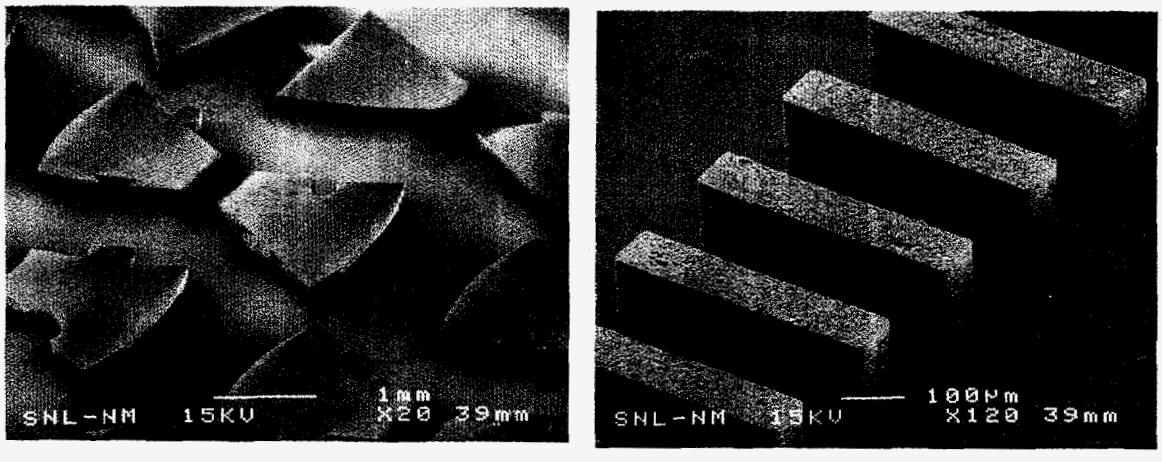

c) d)

Fig. 3 Bonded $Nd_2Fe_{14}B$ micromagnets fabricated using DXRL molding at 200 micron thickness. a) and b) show quadrant shaped geometry which are intended for assembly into a 2 pole-pair permanent magnet rotor. The magnets are magnetized in the direction indicated by the arrow in a). Distortion is present as an artifact of the magnetic field interaction with the SEM imaging and is evident by comparing a) and b) which were taken with different accelerating potentials. c) shows magnet shapes for a 4 pole-pair permanent magnet rotor along with trapezoidal shapes to be used in a magic ring as described in Fig. 8. d) indicates that bar shaped magnets may be processed. Permanent magnet features as small as 5 microns have been replicated at 200 micron structure height.

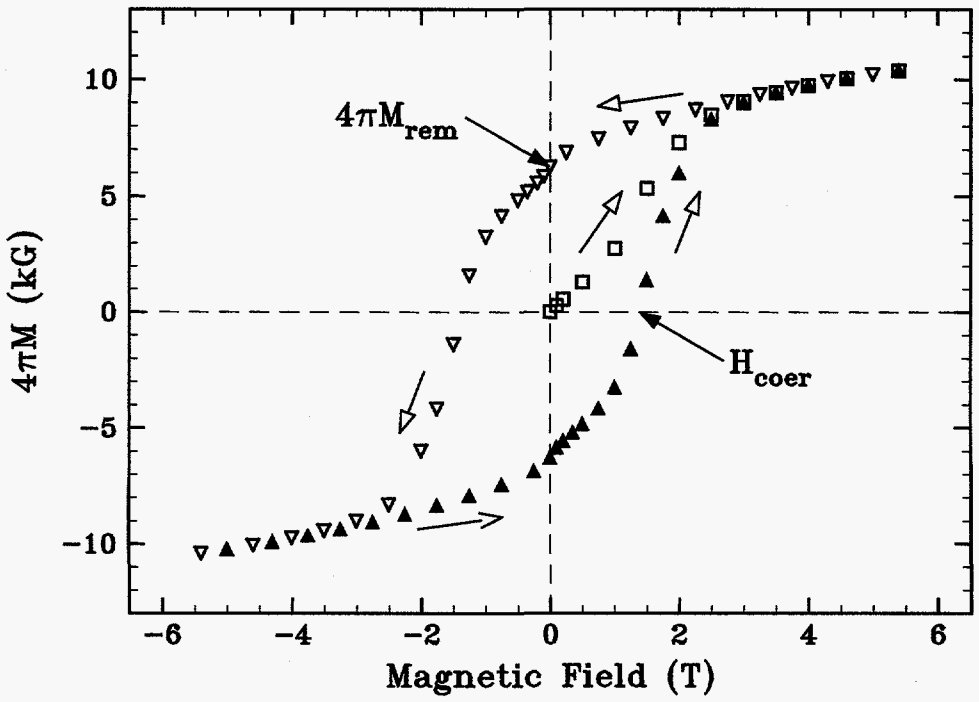

Fig. 4 Full hysteresis loop of bonded isotropic $Nd_2Fe_{14}B$ powder in 20%/vol epoxy with a density of 6.3 g/cm^3. The remanent magnetization is 0.64 T and the coercivity is 1.4 T.

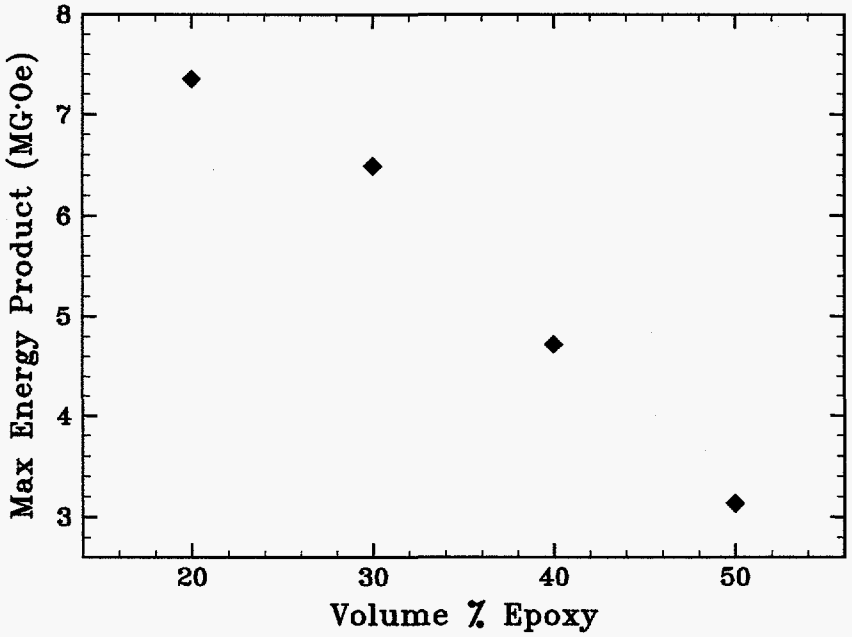

Fig. 5 Maximum energy product as a function of epoxy fraction. An increased epoxy fraction improves the mechanical strength of the permanent magnet.

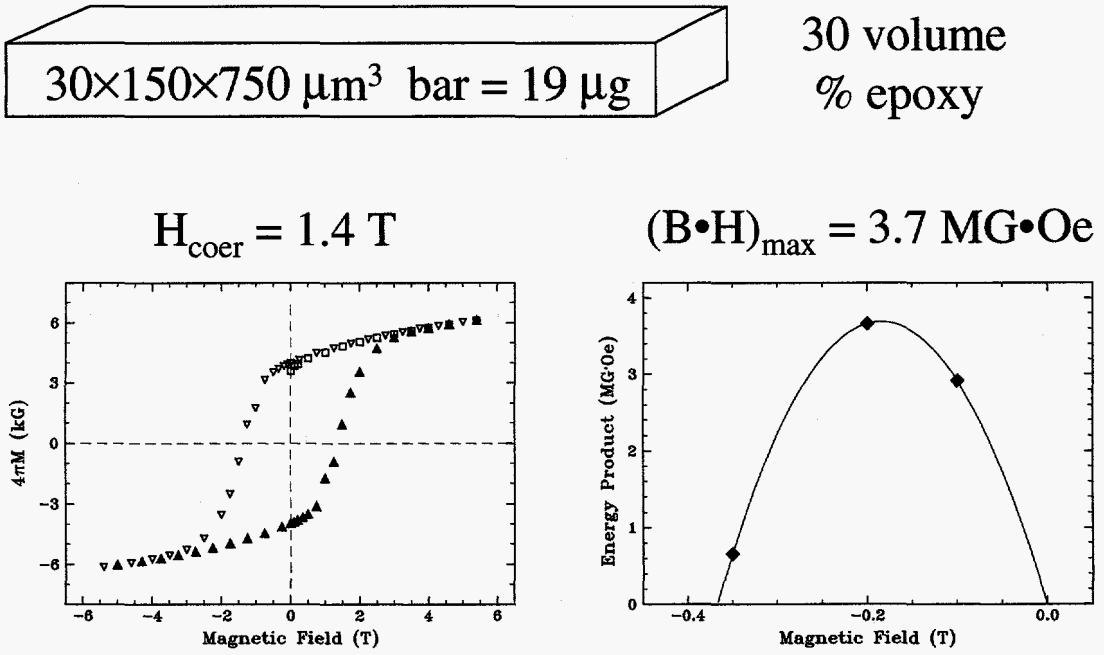

Fig. 6 Data from the smallest permanent magnet which was measured

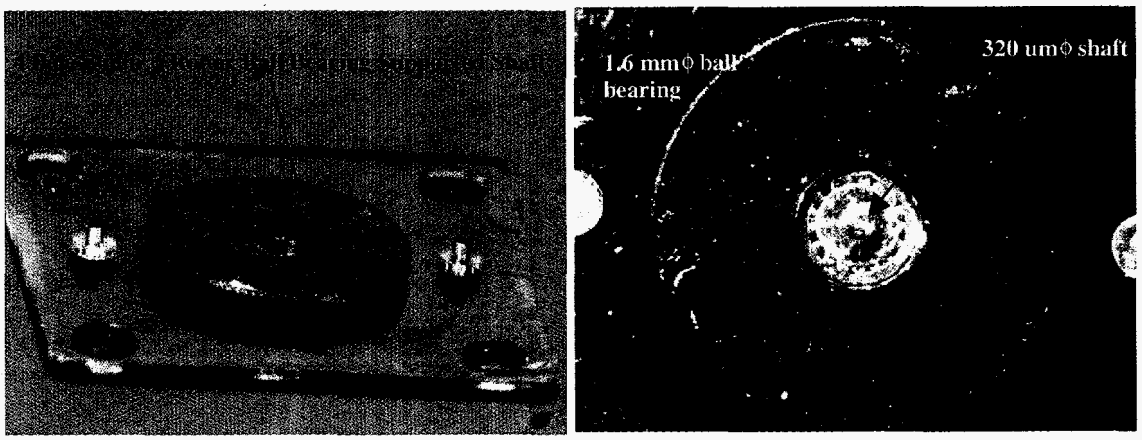

a) b)

Fig. 7 Assembled multipole rotors for brushless DC motor.

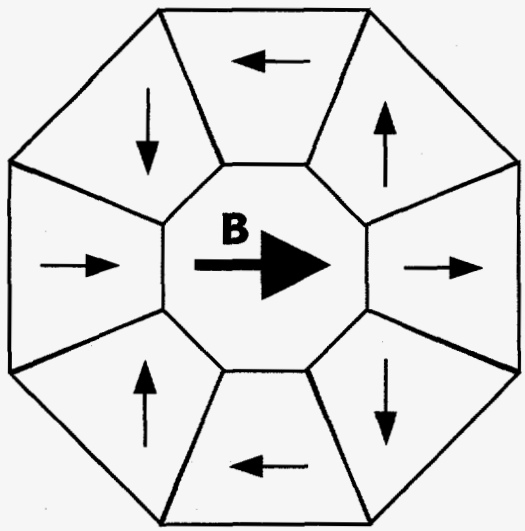

$$\mathbf{B} \rightarrow \mathbf{B}_r \bullet \ln\left(\frac{r_o}{r_i}\right)$$

Fig. 8 Magic ring approximation by discrete permanent magnet elements.

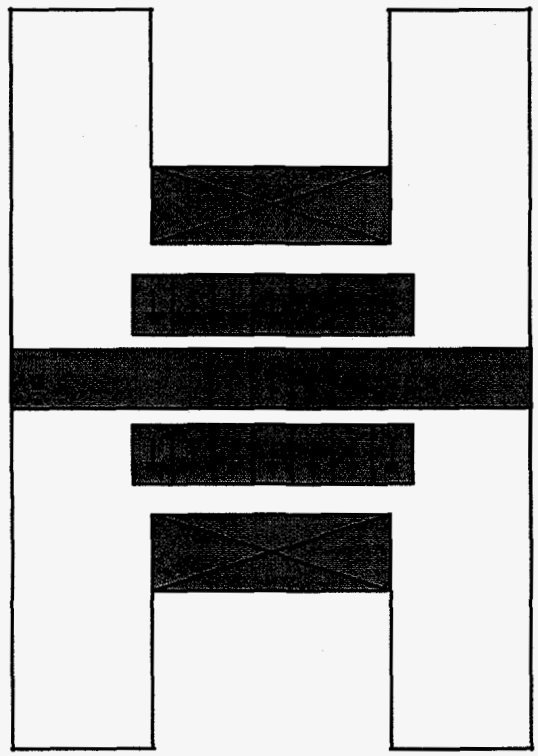

Fig. 9 Schematic diagram demonstrating possible integration of permanent magnets into a "crab-leg" flexure to provide an effectively reduced spring constant.